Materials Chemistry and Physics 124 (2010) 516–528

Contents lists available at ScienceDirect

Materials Chemistry and Physics

journal homepage: www.elsevier.com/locate/matchemphys

Synergetic effects of pulse constraints and additives in electrodeposition of nanocrystalline zinc: Corrosion, structural and textural characterization

M.S. Chandrasekar[a], Shanmugasigamani[b], Malathy Pushpavanam[c,*]

[a] Indian Institute of Technology-Madras, Chennai 36, India
[b] Central Electrochemical Research Institute, Karaikudi 6, India
[c] Alagappa Chettiar College of Engineering and Technology, Karaikudi 6, India

ARTICLE INFO

Article history:
Received 2 March 2010
Received in revised form 8 June 2010
Accepted 5 July 2010

Keywords:
Corrosion test
Electron microscopy (SEM)
Atomic force microscopy (AFM)
Crystallography

ABSTRACT

Pulse electrodeposition was to produce nanocrystalline (nc) zinc from alkaline non-cyanide electrolyte with primary and secondary additives. The combined effect of pulse parameters (ON-time (T_{ON}), OFF-time (T_{OFF}), pulse peak current density (I_P)) and additives on the corrosion properties (evaluated using electrochemical techniques) of zinc electrodeposits are elucidated in terms of surface morphology (using scanning electron microscope), topography and root mean square (RMS) roughness (using atomic force microscope), crystallite size, its orientations and relative texture co-efficient (RTC, %) were evaluated using X-ray diffraction. The corrosion resistance of zinc electrodeposits obtained at constant T_{ON} and I_P enhanced (i.e., low I_{corr} and high R_{ct} values) with increased T_{OFF}. At constant T_{OFF} and I_P, the I_{corr} values increased and R_{ct} values decreased with T_{ON} while the former decreases and latter increases with I_P at constant T_{ON} and T_{OFF}. The inclusion of primary and secondary additives into the electrolyte produced nc zinc electrodeposits at 5 Adm^{-2}, showed enhanced protective properties (I_{corr}—16 $\mu A\,cm^{-2}$ and R_{ct}—481.8 $\Omega\,cm^{-2}$). Fine grained due to high negative overpotential, reduced roughness and higher percentage of basal plane [0 0. 2] orientation have major impact for the enhanced corrosion resistances.

1. Introduction

Nanocrystalline (nc) materials are desirable for a variety of applications as they exhibit impressive properties ranging from high strength and wear resistance, to unique functional characteristics when the grain size approaches ~100 nm or below [1–5]. However, the latter yields a high volume fraction in grain boundaries, which may result in enhanced corrosion performance compared to coarse-grain materials [6–8]. Hence, many efforts have been made in order to refine the grain size of metal deposits and investigate its corrosion behavior.

Many studies have been recently dedicated to the corrosion behavior of nc zinc electrodeposits [9–12]. Zinc deposits are employed to provide good protection to iron and steel components due to its sacrificial nature, low cost and ease of application. Electrodeposition plays a major role compared to other methods to produce zinc coatings. Conventionally adopted cyanide formulations are becoming obsolete due to the increasing health and environmental awareness and more of non-cyanide formulations are being practiced commercially. The alkaline non-cyanide electrolytes have several advantages over the acid baths among which the most important are (1) enhanced corrosion resistance of pure zinc deposits and (2) produce deposits of single-phase alloys with Fe group metals, which also exhibit excellent protective properties [12–14]. Of the various components present in the electrolyte such as salts, buffers and additives, the latter is of importance as they modify the deposition overpotential and nucleation kinetics enabling the production of coatings with particular physical and chemical characteristics (corrosion resistance) [15–17].

Pulse electrodeposition has been found to be a powerful technique for controlling the electrocrystallization process to produce deposits with unique structural and protective properties compared to those obtained by direct current (DC). In former, three independent parameters ON-time (T_{ON}), OFF-time (T_{OFF}) and pulse peak current density (I_P) could be varied [18–21] unlike DC where the only variable is current density [13]. The complexity of pulse electrodeposition process involving large number of experimental variables and shortage of standard route to study the behavior of pulse parameters may produce contradicting results for the same electrode–electrolyte systems. For instances, Youssef et al. stated that longer T_{ON} lead to grain refinement for zinc electrodeposition from zinc-chloride based electrolyte [19]. However, Ramanauskas et al. [11] and Chandrasekar et al. [20] observed

* Corresponding author.
Tel.: +91 4565 227550/227559; fax: +91 4565 227779/227713.
E-mail address: malathypush@yahoo.com (P. Malathy).

0254-0584/$ – see front matter © 2010 Elsevier B.V. All rights reserved.
doi:10.1016/j.matchemphys.2010.07.004

grain-size refinement of zinc deposits (obtained from alkaline non-cyanide electrolyte), with increasing T_{OFF}.

The present paper aimed to study and optimize the synergetic effects of pulse parameters and additives on the corrosion property of zinc electrodeposits obtained from alkaline non-cyanide electrolyte. The causes of latter are substantiated in terms of different morphology, topography and texture obtained due to varying the pulse constraints and additive's concentrations.

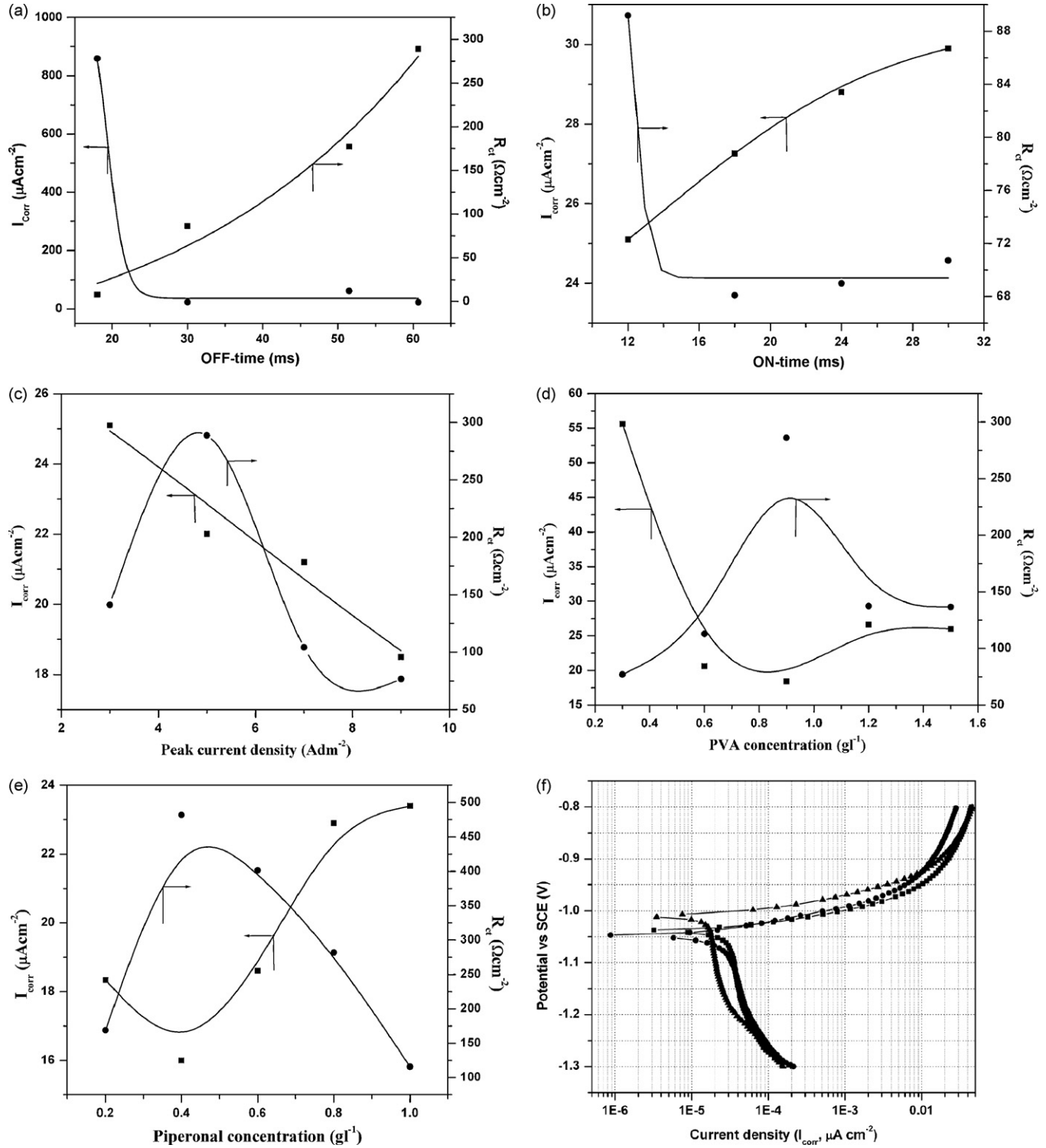

Fig. 1. (a) Effect of pulse OFF-time (T_{OFF}, ms) on I_{corr} (–■–) and R_{ct} (–●–) at constant T_{ON} (6 ms) and I_P (5 Adm^{-2}). (b) Effect of pulse ON-time (T_{ON}, ms) on I_{corr} (–■–) and R_{ct} (–●–) at constant T_{OFF} (60.7 ms) and I_P (5 Adm^{-2}). (c) Effect of pulse current density (I_P, Adm^{-2}) on I_{corr} (–■–) and R_{ct} (–●–) at constant T_{OFF} (60.7 ms) and T_{ON} (6 ms). (d) Effect of polyvinyl alcohol concentration (PVA, g l^{-1}) on I_{corr} (–■–) and R_{ct} (–●–) at constant T_{OFF} (60.7 ms), T_{ON} (6 ms) and I_P (5 Adm^{-2}). (e) Effect of piperonal concentration (PIP, g l^{-1}) on I_{corr} (–■–) and R_{ct} (–●–) at constant T_{OFF} (60.7 ms), T_{ON} (6 ms), I_P (5 Adm^{-2}) and PVA (0.9 g l^{-1}) concentration. (f) Typical potentiodynamic polarization curves at constant T_{OFF} (60.7 ms), T_{ON} (6 ms), I_P (5 Adm^{-2}): (–■–) without additive, (–●–) 0.9 g l^{-1} PVA, (–▲–) 0.4 g l^{-1} piperonal + 0.9 g l^{-1} PVA concentration. (g) Typical AC impedance curves at constant T_{OFF} (60.7 ms), T_{ON} (6 ms), I_P (5 Adm^{-2}): (–●–) without additive, (–■–) 0.9 g l^{-1} PVA, (–▲–) 0.4 g l^{-1} piperonal + 0.9 g l^{-1} PVA concentration. Inset is its equivalent circuit model.

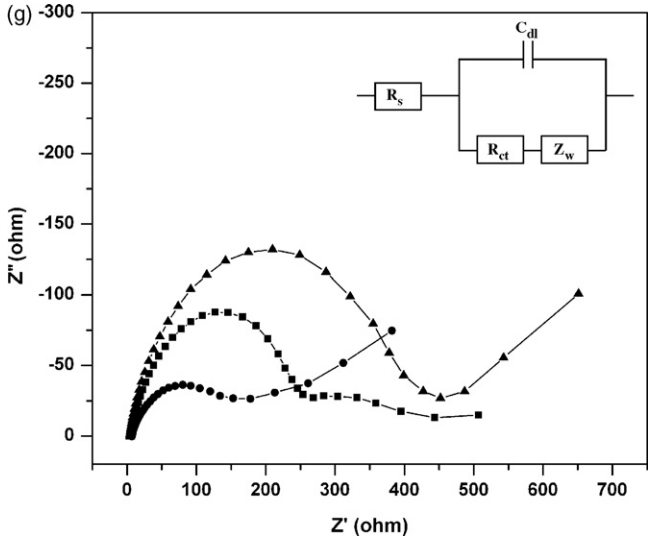

Fig. 1. (*Continued*)

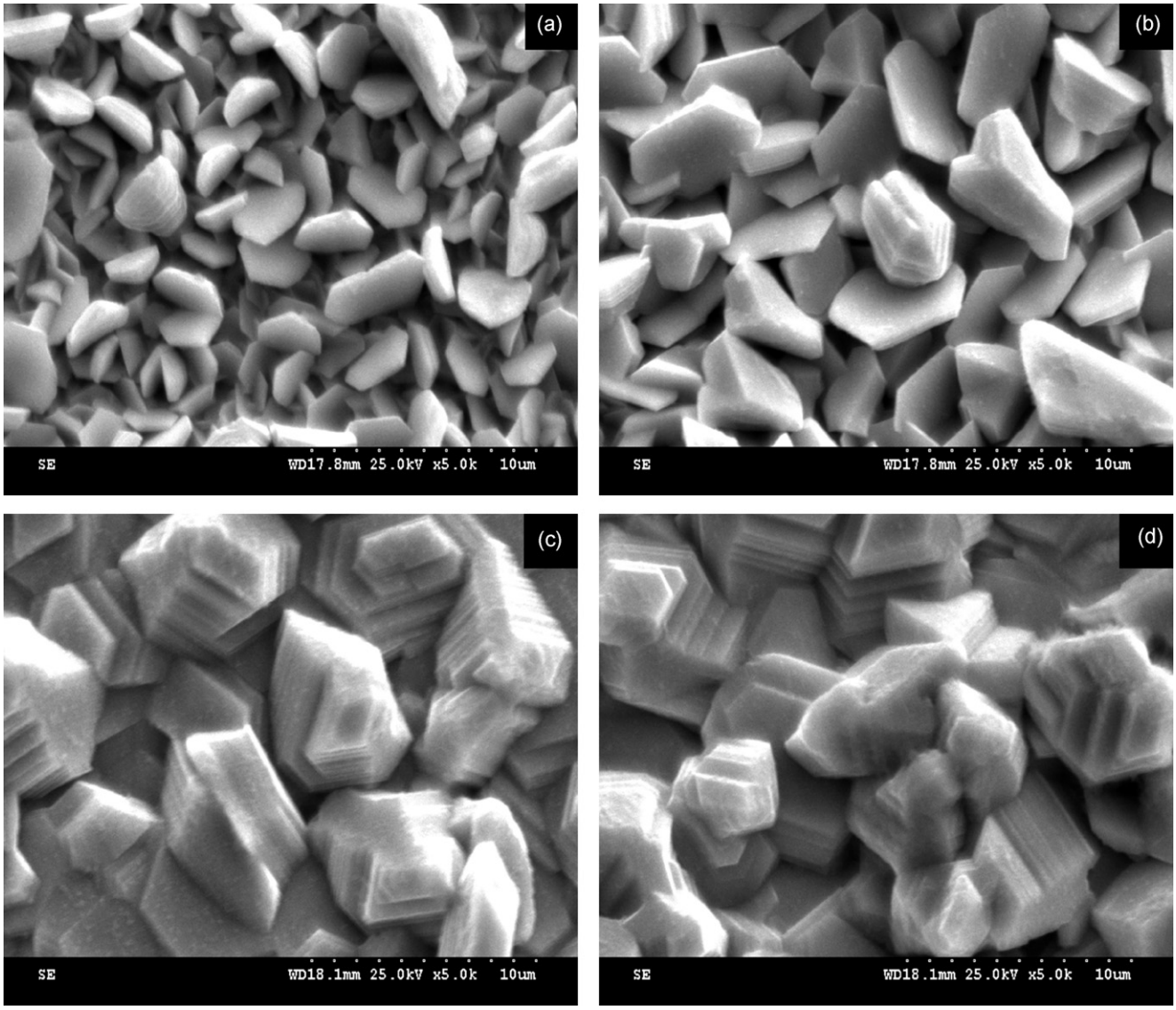

Fig. 2. SEM images of the surface morphology of zinc deposits obtained at constant T_{ON} (6 ms), I_P (5 Adm^{-2}) and different T_{OFF} of (a) 18 ms, (b) 30 ms, (c) 51.5 ms, and (d) 60.7 ms.

2. Experimental

2.1. Electrolyte and electrolytic cell

An alkaline non-cyanide electrolyte contained ZnO 10–12 g l^{-1}, NaOH 90–120 g l^{-1} and organic additives [13,20] was prepared with due pretreatments using (60 g l^{-1} zinc dust activated with 0.1 ml of 50% HCl) to remove the metallic and organic impurities [22–24]. The primary additive was prepared by dissolving 400 g of latter in 300 ml of water with constant heating while secondary additive prepared by dissolving 30 g in 100 ml methanol.

Pulse electrodeposition was carried out in a 175 ml capacity cell. Mild steel plates were used as cathode with 2 cm × 2 cm (exposed area) and (99.99% pure, Aldrich)

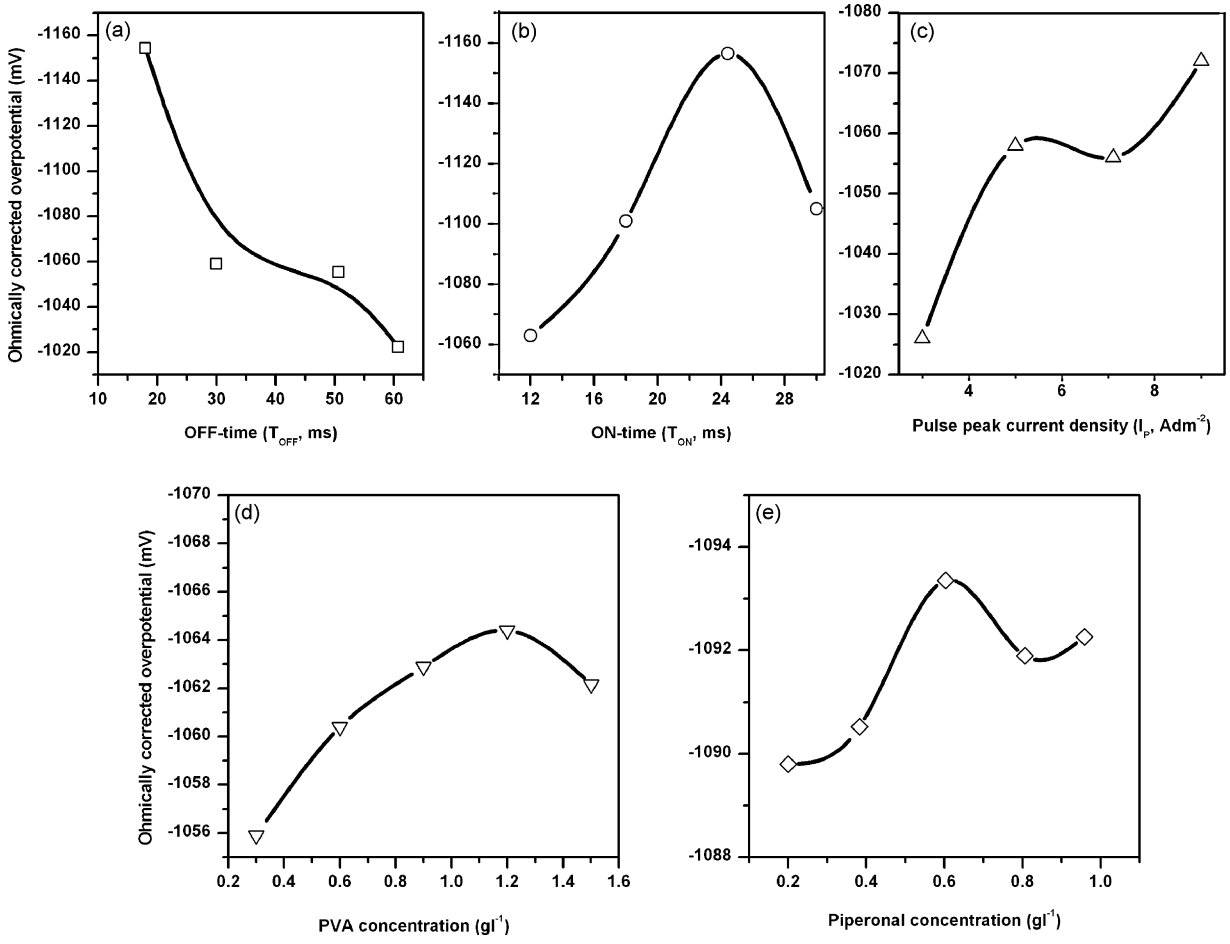

Fig. 3. Effect of pulse parameters and additives on ohmically corrected overpotential: (–□–) T_{OFF} (ms) at constant T_{ON} (6 ms) and I_P (5 Adm^{-2}); (–○–) T_{ON} (ms) at constant T_{OFF} (60.7 ms) and I_P (5 Adm^{-2}); (–△–) I_P (Adm^{-2}) at constant T_{OFF} (60.7 ms) and T_{ON} (6 ms); (–▽–) PVA (g l^{-1}) at constant T_{OFF} (60.7 ms), T_{ON} (6 ms) and I_P (5 Adm^{-2}); (–◇–) piperonal concentration at constant T_{OFF} (60.7 ms), T_{ON} (6 ms), I_P (5 Adm^{-2}) and PVA (0.9 g l^{-1}) concentration.

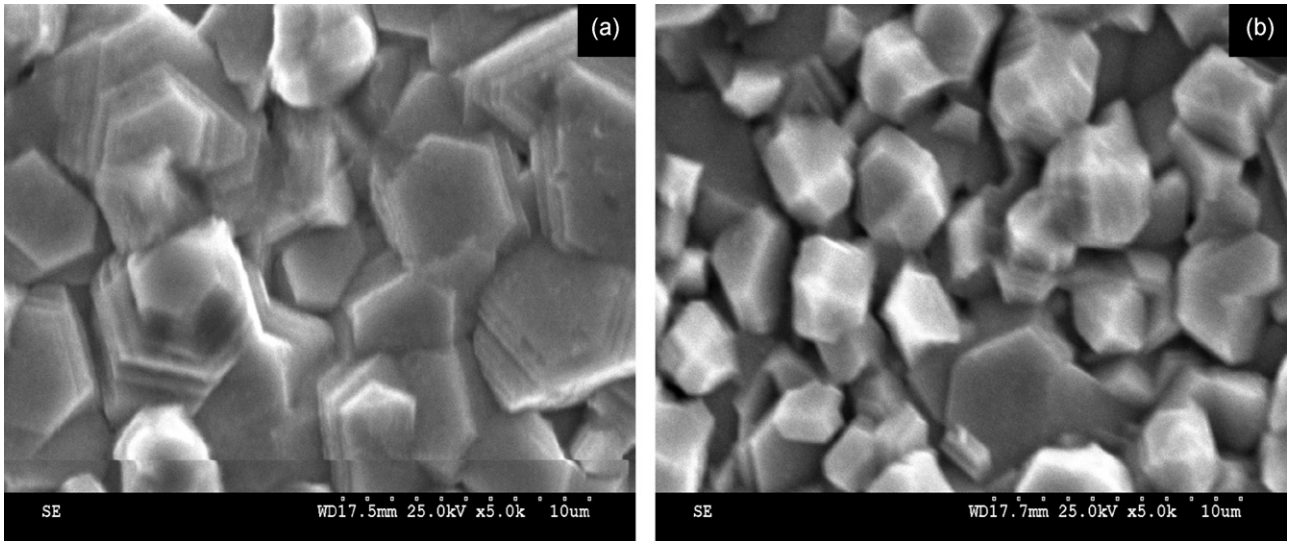

Fig. 4. SEM images of the surface morphology of zinc deposits obtained at constant T_{OFF} (60.7 ms), I_P (5 Adm^{-2}) and different T_{ON} of (a) 12 ms and (b) 18 ms.

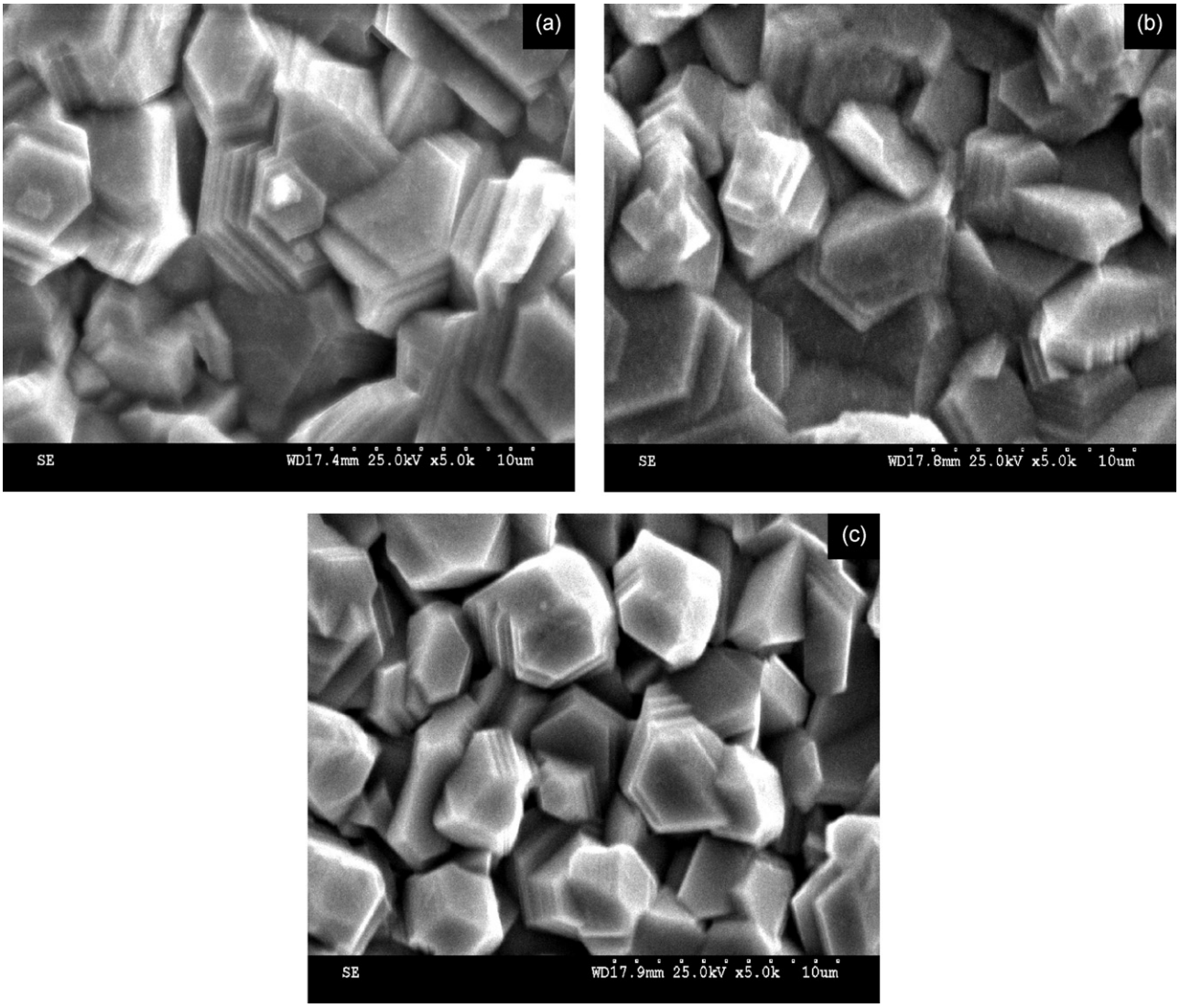

Fig. 5. SEM images of the surface morphology of zinc deposits obtained at constant T_{ON} (6 ms), T_{OFF} (60.7 ms) and different I_P of (a) 3 Adm^{-2}, (b) 5 Adm^{-2}, and (c) 7 Adm^{-2}.

zinc sheet as a soluble anode to obtain 5 μm thick zinc deposit. Before electrodeposition, the mechanically polished, mirror bright steel plates were cleaned with trichloroethylene and given cathodic and anodic cleaning for 120 and 30 s respectively in the conventional alkaline cleaner solution (containing 35 $g\,l^{-1}$ NaOH and 25 $g\,l^{-1}$ Na_2CO_3). All chemicals used were of Laboratory Grade, supplied by Merck or Fischer.

All electrodeposition experiments were carried out at room temperature (30–35 °C). The cathode current efficiency (CCE %) was calculated from the mass gain obtained after deposition and found to vary between 60% to 85%.

2.2. Pulse electrodeposition

A DC regulated pulse power rectifier (Saral Systems, model: PR 1010 TPS, India) was used to generate the square pulse waveforms. Measured uncompensated ohmic resistance (R) was used to calculate the uncompensated ohmic potential drop (IR) between working and reference electrodes. The ohmically corrected overpotential was determined by deducting the open-circuit potential (OCP) from the ohmically corrected working electrode potential. The coatings were obtained by varying the T_{OFF} from 6 to 60.7 ms, T_{ON} from 6 to 30 ms and I_P from 3 to 9 Adm^{-2}. The effect of each pulse parameter on the deposit quality and corrosion properties was studied maintaining the other two at standard conditions: T_{OFF}, 60.7 ms; T_{ON}, 6 ms and I_P, 5 Adm^{-2}.

2.3. Corrosion studies: cell assembly and electrolyte

A three-necked cell of 50 ml capacity was used. The working electrode was electrodeposited zinc on steel plate with exposed area of 1 cm^2 with a platinum counter electrode and a saturated calomel (SCE) reference electrode. 5 wt.% NaCl solution was used as electrolyte. Corrosion tests were conducted at room temperature.

Potentiodynamic polarization and alternating current (AC) impedance studies were carried out using BAS-ZAHNEER IM6 Impedance Analyzer and results were analyzed using Thales 3.18USB software. The electroplated zinc was introduced into cell immediately and allowed to reach equilibrium, which usually took 8–12 min. Potentiodynamic polarization was obtained at a scan rate of 5 $mV\,s^{-1}$ and the corrosion potential (E_{corr}) and corrosion current density (I_{corr}) were determined using the Tafel extrapolation method. Impedance measurements were made at the frequency range of 50 mHz to 100 kHz with 10 mV peak amplitude about the corrosion potential.

2.4. Characterization of zinc electrodeposits

A scanning electron microscope (SEM) (Hitachi, model: S3000H, Canada) and atomic force microscope (AFM) (Molecular Imaging Scanning Probe Microscope, model: PICOSPM, US) were used to characterize the surface morphology and topography of zinc electrodeposits, respectively. In latter, Si_3N_4 cantilever was used to obtain images of 256 × 256 pixels resolution. Molecular Imaging SPM Lab grain analysis software and AFM image profile line analysis were employed to determine grain size of electroplated zinc coatings. The grain size of zinc platelets was calculated by averaging the length, width and thickness of each platelet observed and the RMS roughness values were determined on the basis of AFM studies.

X-ray diffraction (XRD) measurements were performed with X'PERT PRO PANalytical (model: PW3040 160 X'Pert PRO, Netherlands) equipped with Cu Kα

radiation. Crystallite size was estimated by Scherrer's equation [17]. Relative texture co-efficient (RTC, %) of the zinc electrodeposits was calculated from XRD datas according to the method proposed by Berube and L'Esperance [25].

3. Results and discussion

3.1. Corrosion studies

The protective properties of pulsed zinc coatings were studied using potentiodynamic polarization and AC impedance techniques in 5 wt.% NaCl solution [20]. For all experiments, OCP (open-circuit potential) shown variation from −1.01 to −1.05 V while rest potential (R_P) ranged between −1.06 to −1.07 V. The corrosion properties of pulse electrodeposited zinc produced at each pulse parameters and various additive concentrations were experimented. These parameters were optimized based on the low corrosion current density (I_{corr}), and high resistance to charge transfer (R_{ct}).

Fig. 1a shows the effect of T_{OFF} on the I_{corr} and R_{ct} at constant T_{ON} (6 ms) and I_P (5 Adm^{-2}). The I_{corr} values decreased from 859 to 22 μA cm^{-2} while R_{ct} values increased from 7.65 to 288.78 Ω cm^{-2} exhibiting enhanced corrosion protection with increasing T_{OFF}. Fig. 1b depicts that at constant T_{OFF} (60.7 ms) and I_P (5 Adm^{-2}), the I_{corr} values increased from 25 μA cm^{-2} at 12 ms (T_{ON}) to 30 μA cm^{-2} at 30 ms (T_{ON}) while R_{ct} values decreased from 89.2 to 70.71 Ω cm^{-2}, showing less protective ability compared to T_{ON} of 6 ms (I_{corr} = 22 μA cm^{-2} and R_{ct} = 288.78 Ω cm^{-2}). Moreover, the zinc electrodeposits obtained with increasing I_P (between 3 and 9 Adm^{-2}) at constant T_{ON} (6 ms) and T_{OFF} (60.7 ms) showed enhanced protective property as shown in Fig. 1c. This is substantiated with R_{ct} values decreasing from 25.1 μA cm^{-2} (at 3 Adm^{-2}) to 18.5 μA cm^{-2} (at 9 Adm^{-2}) while C_{dl} value increased to 288.78 Ω cm^{-2} (at 5 Adm^{-2}) and then decreases. Hence, 5 Adm^{-2} is optimized for the rest of the experiments since this condition provide enhanced corrosion resistance compared to other I_P (Fig. 1c). The I_{corr} values of zinc

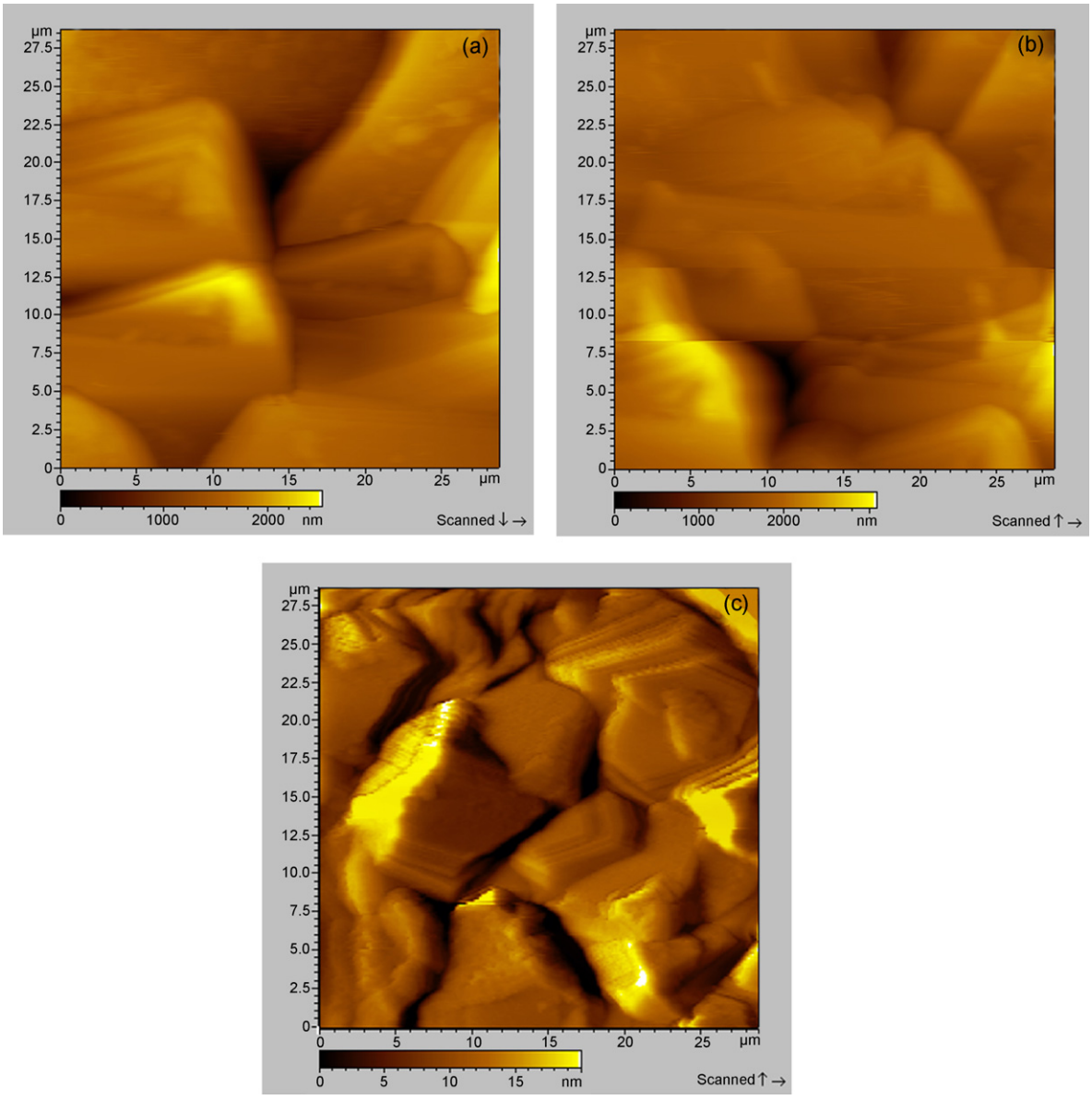

Fig. 6. AFM images of pulsed zinc coatings at constant T_{ON} (6 ms), T_{OFF} (60.7 ms) and different I_P of (a) 3 Adm^{-2}, (b) 5 Adm^{-2}, and (c) 7 Adm^{-2}.

deposits obtained with inclusion of primary additive (polyvinyl alcohol, PVA) and secondary additive (piperonal) into the electrolyte at optimized pulse parameters of 6 ms (T_{ON}), 60.7 ms (T_{OFF}) and 5 Adm^{-2} (I_P) are shown in Fig. 1d–f. Zinc deposit obtained at 0.9 g l^{-1} PVA concentration, exhibited 18.4 μA cm^{-2} (I_{corr}) and 278.13 Ω cm^{-2} (R_{ct}) while deposits obtained with electrolyte containing 0.4 g l^{-1} piperonal + 0.9 g l^{-1} PVA exhibited lowest I_{corr} value of 16 μA cm^{-2} and highest R_{ct} value of 481.8 Ω cm^{-2}.

The Nyquist impedance plots for zinc electrodeposit obtained with and without additives at 6 ms (T_{ON}), 60.7 ms (T_{OFF}) and 5 Adm^{-2} (I_P) are in Fig. 1g. The Nyquist plots of all the zinc deposits studied exhibit a single semicircle at higher frequencies; however, the diameter of the latter is sharply increased with inclusion of

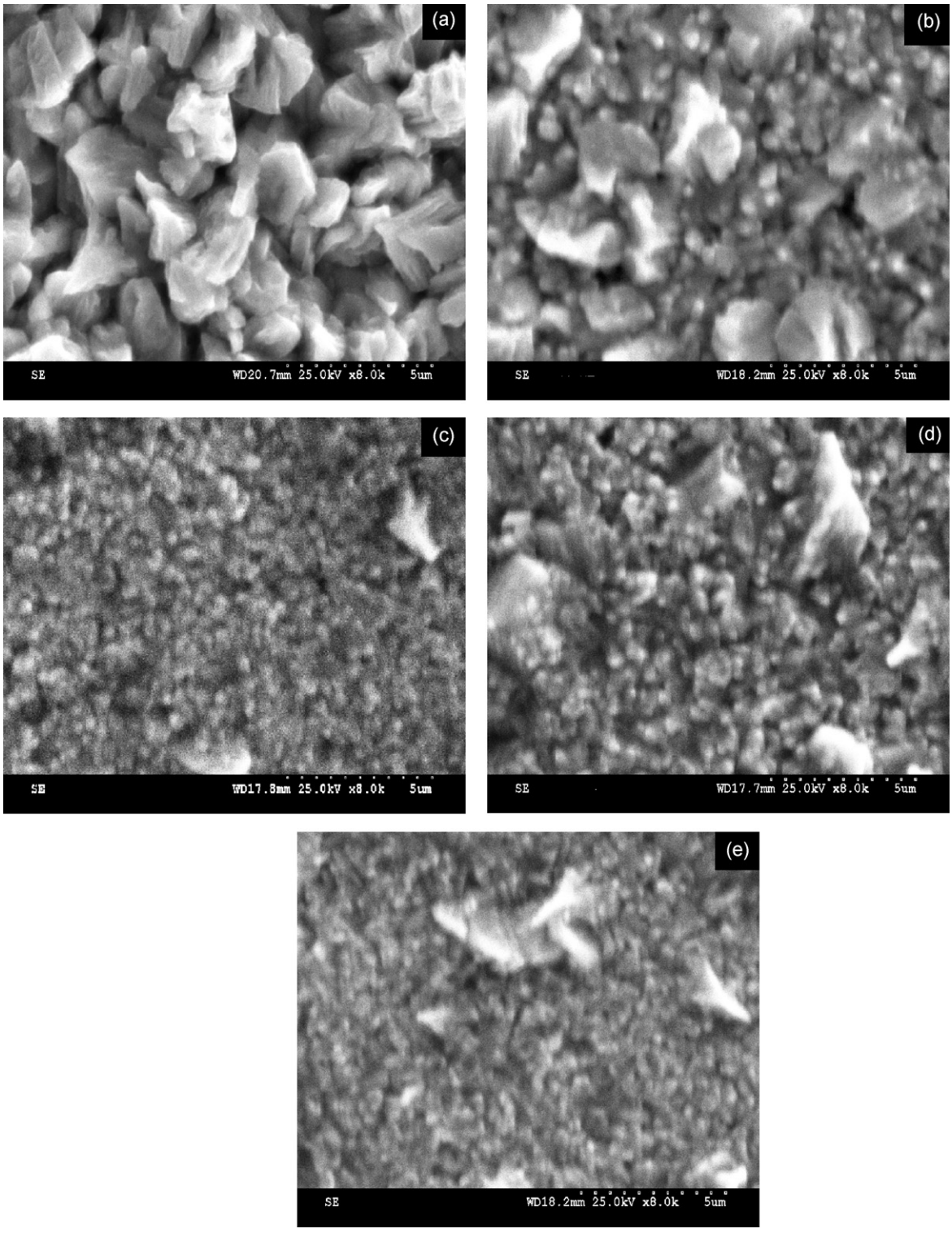

Fig. 7. SEM images of the surface morphology of zinc deposits obtained at constant T_{ON} (6 ms), T_{OFF} (60.7 ms), I_P (5 Adm^{-2}) and different PVA concentrations of (a) 0.3 g l^{-1}, (b) 0.6 g l^{-1}, (c) 0.9 g l^{-1}, (d) 1.2 g l^{-1}, and (e) 1.5 g l^{-1}.

additives. This is indicative of much higher corrosion resistance of zinc coatings. In addition, a diffusion controlled charge transfer is observed at low frequencies, as depicted in Fig. 1g. Such a diffusion process may indicate that the corrosion mechanism is controlled not only by the charge transfer step but also by the diffusion process. To account for the corrosion behavior of the zinc deposits, an equivalent circuit model consists of solution resistance (R_s) double layer capacitance (C_{dl}), charge transfer resistance (R_{ct}) and Warburg impedance (Z_w) [26], in which the C_{dl} and R_{ct} are parallel to each other, have been proposed to simulate the metal/solution interface [10]. Youssef et al. reported that the passive film formation on the corroded zinc surface to be diffusion controlled and the enhanced corrosion protection is believed due to the high nucleation density sites for passive films [10].

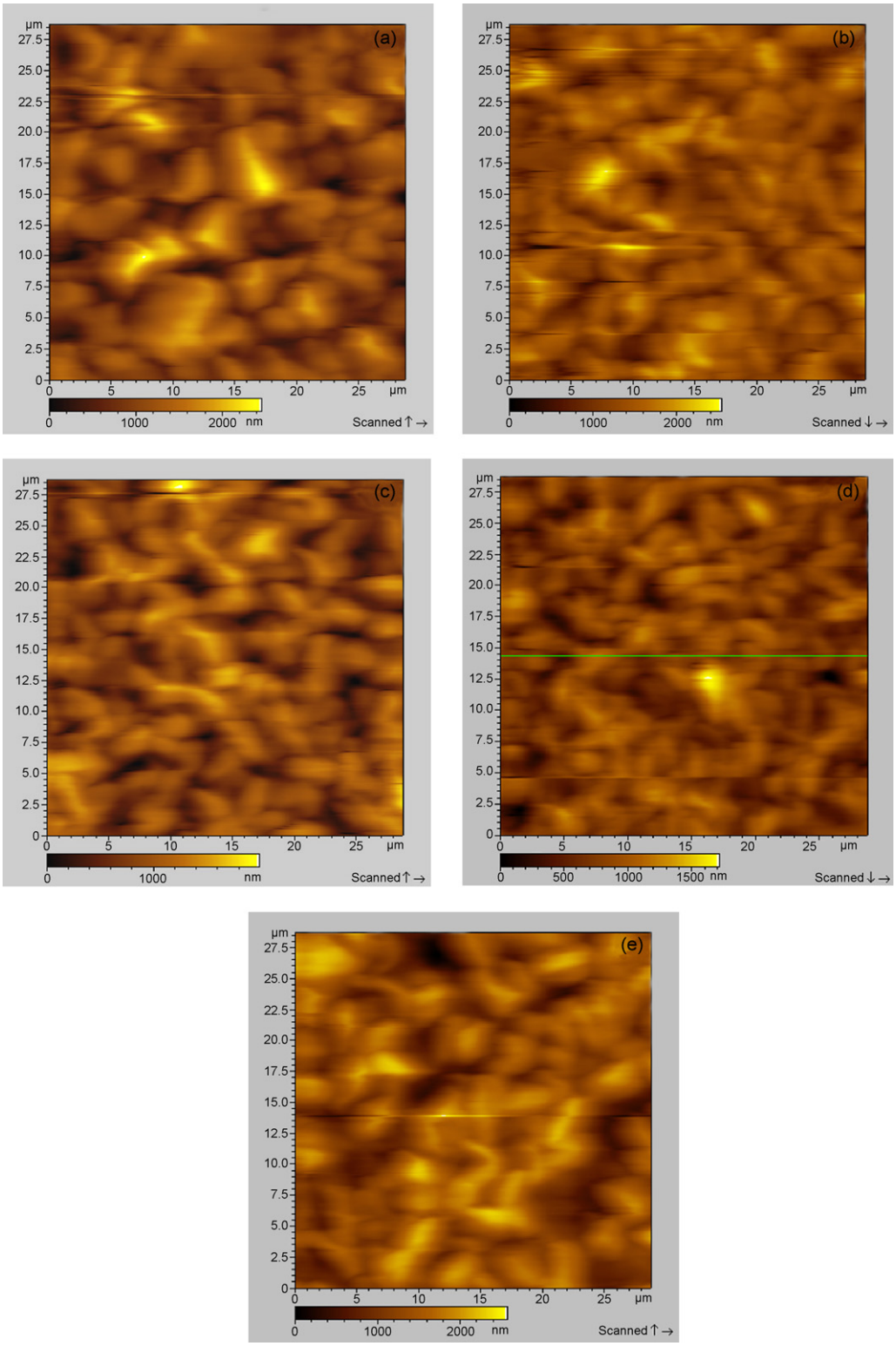

Fig. 8. AFM images of pulsed zinc coatings at constant T_{ON} (6 ms), T_{OFF} (60.7 ms), I_P (5 Adm^{-2}) and different PVA concentrations of (a) 0.3 g l^{-1}, (b) 0.6 g l^{-1}, (c) 0.9 g l^{-1}, (d) 1.2 g l^{-1}, and (e) 1.5 g l^{-1}.

The above corrosion protection ability of pulsed zinc electrodeposits were elucidated in terms of morphology, topography, root mean square (RMS) roughness and preferred orientation.

3.2. Morphology and topography

Surface morphology and topography of zinc electrodeposits are based on SEM and AFM measurements, respectively. SEM, AFM

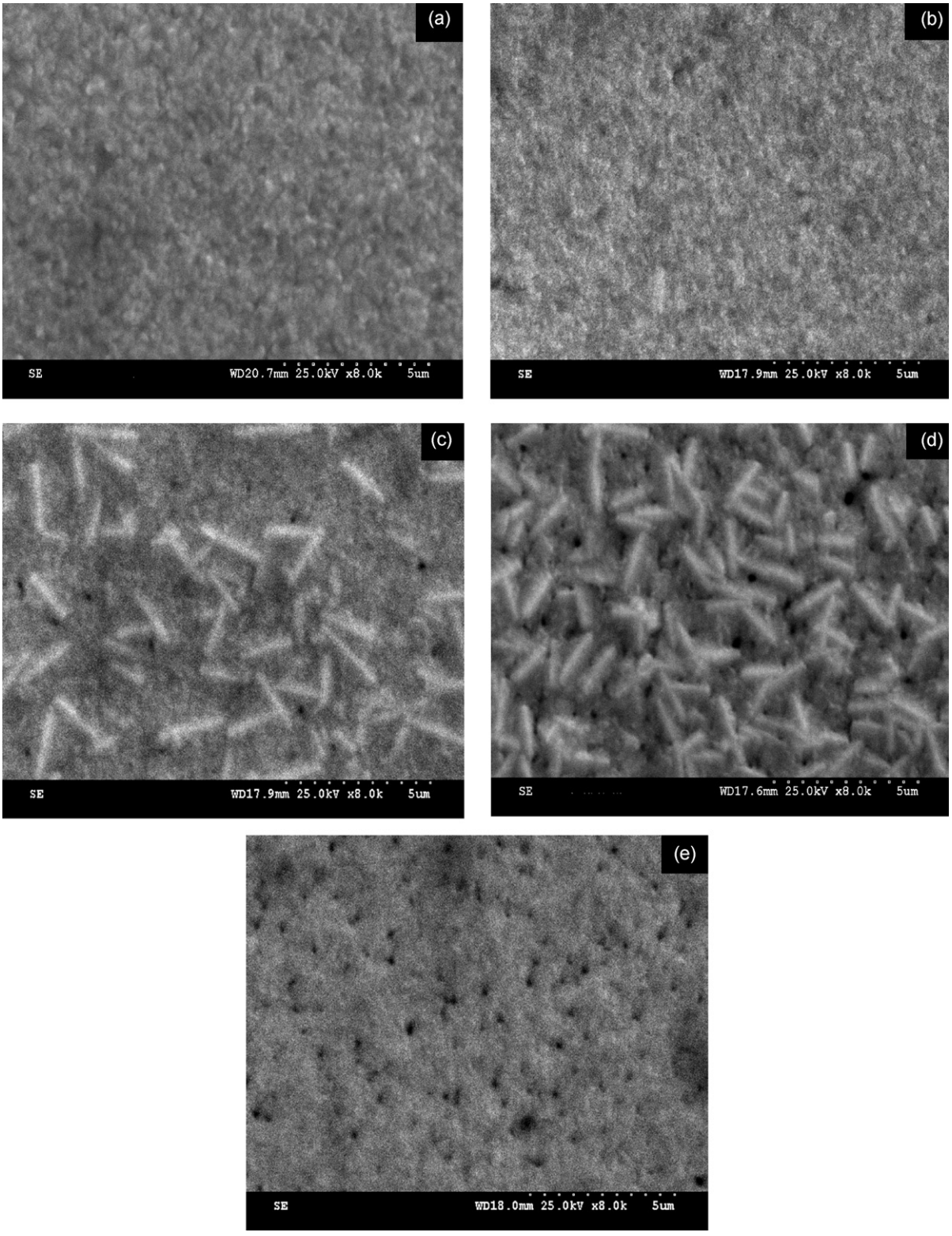

Fig. 9. SEM images of the surface morphology of zinc deposits obtained at constant T_{ON} (6 ms), T_{OFF} (60.7 ms), I_P (5 Adm^{-2}), PVA concentration (0.9 g l^{-1}) and different piperonal concentrations of (a) 0.2 g l^{-1}, (b) 0.4 g l^{-1}, (c) 0.6 g l^{-1}, (d) 0.8 g l^{-1}, and (e) 1.0 g l^{-1}.

micrographs and overpotential representing the effects of pulse plating parameters and additives are shown in Figs. 2–10. Influences of pulse constraints and additives on grain size and its distribution and RMS roughness are determined based on these studies.

Hexagonal flake-shaped platelets were obtained at 18 and 30 ms (T_{OFF}) as shown in Fig. 2a and b. These platelets of reduced dimensions stacked at 51.5 and 60.7 ms (T_{OFF}) (Fig. 2c and d). This might be due to the adsorption of an inhibiting species probably the hydroxyl anion, which blocks the growth centers of the cathode and enhance new nuclei at each pulse. Therefore, longer the T_{OFF}, finer would be the platelets which pile together. Another plausible explanation for latter may be due to the lower overpotential associated with increasing T_{OFF} (Fig. 3a). Meanwhile, increase in T_{ON} (=12 ms) increases the stack size (Fig. 4a). According to pulse plating theory, the thickness of the pulsating part of diffusing layer is a function

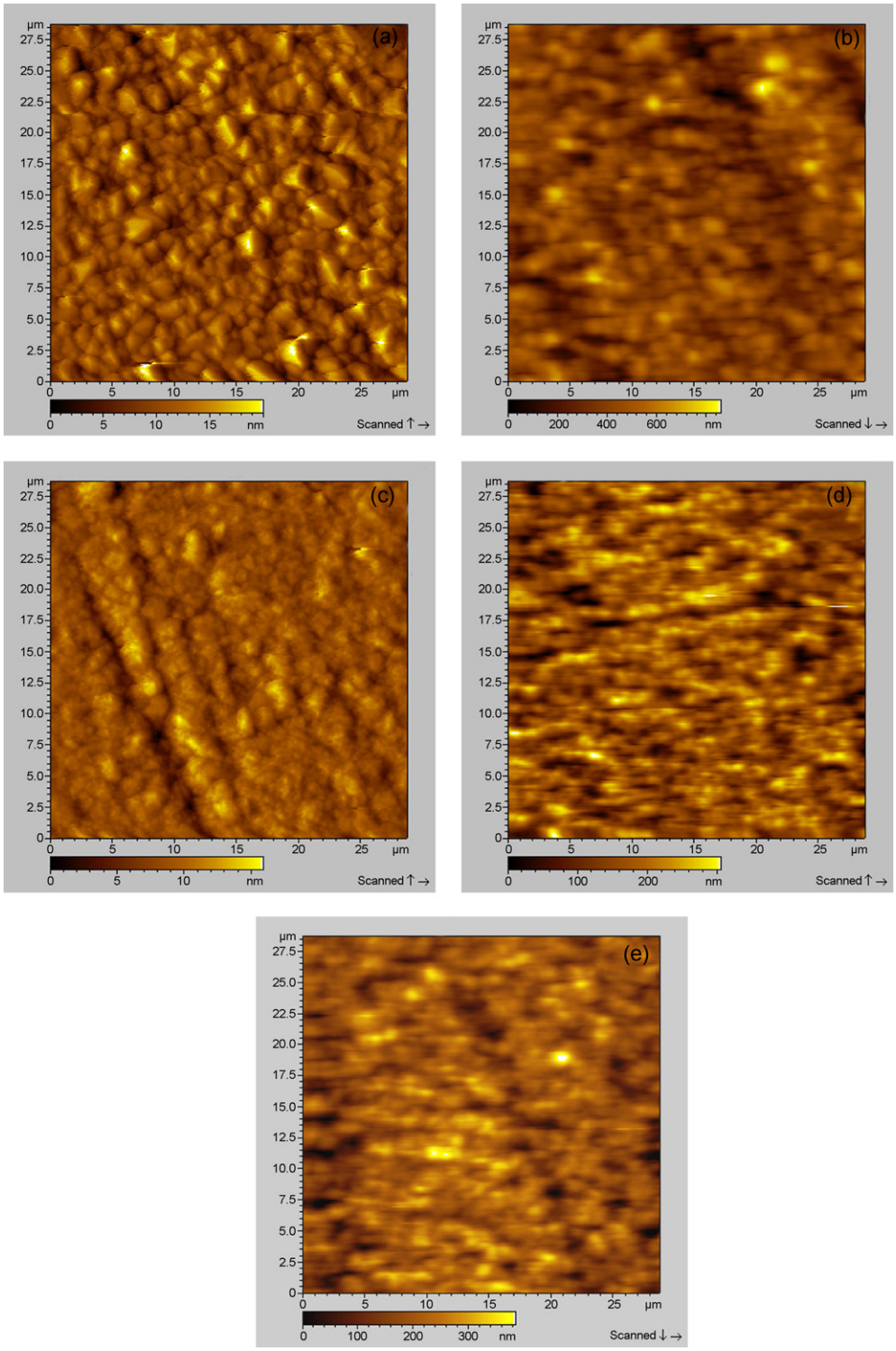

Fig. 10. AFM images of pulsed zinc coatings at constant T_{ON} (6 ms), T_{OFF} (60.7 ms), I_P (5 Adm^{-2}), PVA concentration (0.9 g l^{-1}) and different piperonal concentrations of (a) 0.2 g l^{-1}, (b) 0.4 g l^{-1}, (c) 0.6 g l^{-1}, (d) 0.8 g l^{-1}, and (e) 1.0 g l^{-1}.

of T_{ON}. If the diffusing layer's thickness is small compared to the surface roughness of the base metal, which is possible at sufficiently short T_{ON}, compact deposits are formed. Further, increase in T_{ON} (=18 ms), decreases the stack size (Fig. 4b), might be due to increase in overpotential associated with T_{ON} (Fig. 3b). These results of T_{OFF} and T_{ON} effects are in contradicting with Youssef et al. [19] who produced nc zinc from chloride–sulfate electrolyte. Hence, with increase in T_{OFF}, the stack size decrease from 3.5 to 1.5 μm that might result in decrease of I_{corr} and increase (resistance to charge transfer) R_{ct} values. With increase in T_{ON}, the stack size increased from ~2.8 to 2.82 μm which may contribute to high I_{corr} and decreased R_{ct} values.

Fig. 5 depicts that increase in I_P increases the overpotential (Fig. 3c), which results in decreases of stack size. These results are consistent with the results obtained by a number of investigators [21,29,30]: increasing the overpotential increases the free energy to form new nuclei, which results in a higher nucleation rate and smaller grain size. Surface topography investigations on the μm level (30 μm × 30 μm scanned surface area) have shown that zinc deposits consisted of micron sized granular crystallite agglomerations (Fig. 6a–c). The average dimensions of these agglomeration being ~1.45 μm. The average RMS roughness for zinc deposits (with 30 μm × 30 μm scanned surface area) was ~530 nm.

We observed that another contribution for increasing the (more negative) overpotential resulted from addition of additives. The addition of primary additive namely, polyvinyl alcohol (PVA) into electrolyte modify the morphology along with reduction of grain size (Fig. 7a–e). These might be due to (1) polarity of the carbon–oxygen bond and (2) possibility of this material to be present in significant amounts in the cathode film, forming a weak physical barrier that hinders zinc deposition. The grain refining properties of PVA could be due to (1) the energy needed to break the PVA complex at cathode and (2) increase in overpotential with its concentration (Fig. 3d). The grain size decreased from ~1.2 to ~150 nm (Fig. 8a–e). At 0.9 g l^{-1} PVA, 5 A dm^{-2} (I_P), 60.7 ms (T_{OFF}), 6 ms (T_{ON}), nc zinc deposit (~50 nm) was obtained while the average RMS roughness (with 30 μm × 30 μm scanned surface area) was ~350 nm. To obtain bright zinc deposits from this bath, additional organic brighteners are needed in addition to PVA. These organic brighteners are smaller molecules having unsaturated and polar characteristics by which they are attracted to the cathode and influence the deposition [13,27,28]. The role of brightener additives is to further refine the structure or produce leveling by selective adsorption and to the surface film formed by PVA. Piperonal, an aldehyde is of such a brightener additive. The bright, compact and adherent zinc deposits were obtained with inclusion of piperonal to electrolyte containing 0.9 g l^{-1} PVA (Fig. 9). At 0.4 g l^{-1} piperonal concentrations, nc zinc deposit containing grain size of ~33 nm was obtained (Fig. 10b). This could be due to increase in overpotential associated with increase in piperonal concentrations (Fig. 3e). Further increase in its concentrations results in porous deposits containing numerous pits (Fig. 10d and e). The average RMS roughness for zinc deposits with brightener additive (with 30 μm × 30 μm scanned surface area) was ~200 nm.

Zinc coatings produced at 6 ms (T_{ON}), 60.7 ms (T_{OFF}), 5 A dm^{-2} (I_P), 0.9 g l^{-1} PVA + 0.4 g l^{-1} piperonal concentrations have shown enhanced protective property compared to other I_P and additive's concentrations. The corrosion resistances observed at different additive concentrations were attributed to differences in morphology, topography, RMS roughness (Fig. 11) and grain size of the zinc deposits. Compact, adherent and more homogeneous structure (more uniform agglomeration/grain size) might be plausible explanation for low I_{corr} (16 μA cm^{-2}), high R_{ct} (447.26 Ω cm^{-2}) and low C_{dl} (12.6 μF cm^{-2}) values. Hence, the relationship between the structural parameters and corrosion behavior were regular.

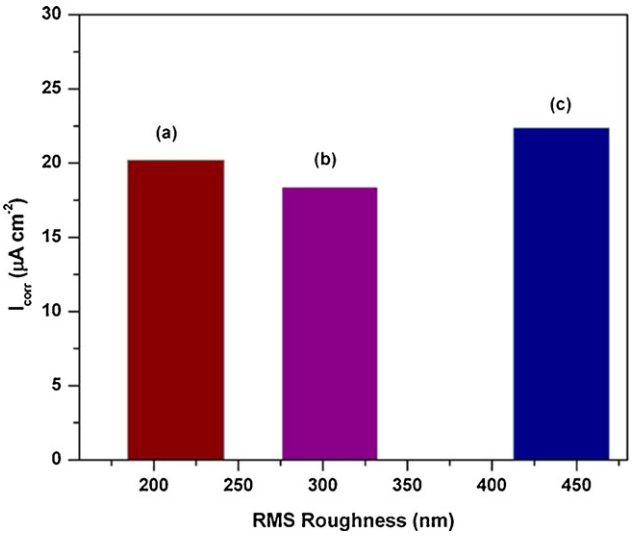

Fig. 11. Typical effect of root mean square (RMS) roughness on corrosion current density (I_{corr}): (a) T_{ON} (6 ms), T_{OFF} (60.7 ms), I_P (5 A dm^{-2}), 0.9 g l^{-1} PVA; (b) T_{ON} (6 ms), T_{OFF} (60.7 ms), I_P (5 A dm^{-2}), 0.9 g l^{-1} PVA + 0.4 g l^{-1} PIP; (c) 6 ms (T_{ON}), 60.7 ms (T_{OFF}), 5 A dm^{-2} (I_P).

3.3. Crystallographic orientation

Different crystallographic orientations of zinc polycrystalline grains might have effect on corrosion rates. The activation energy for dissolution increases with increase in packing density. In such a case, the plane with the highest packing density must have the lowest corrosion rates and the packing density of zinc crystallographic planes decreases in the following order [0 0. *l*] > [*h k*. 0] > [*h* 0. 0] [31]. Furthermore, it was shown that the growth of zinc oxide (ZnO) films on zinc surfaces is dependent upon the index of the specific plane [32]. The integrity of the oxide film on the basal [0 0. *l*] plane of zinc surface, relative to other orientations was attributed to be quite protective [33]. Therefore, the deposits, that possessed a low-index plane texture, might be more stable due to a higher metal packing density and due to the fact that oxide films on such surfaces were more resistant.

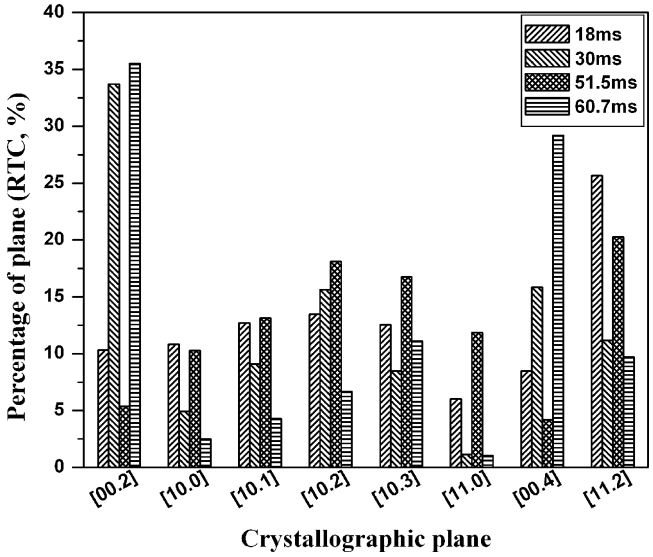

Fig. 12. Percentage RTC as a function of crystallographic planes at constant T_{ON} (6 ms), I_P (5 A dm^{-2}) and different T_{OFF} of (a) 18 ms, (b) 30 ms, (c) 51.5 ms, and (d) 60.7 ms.

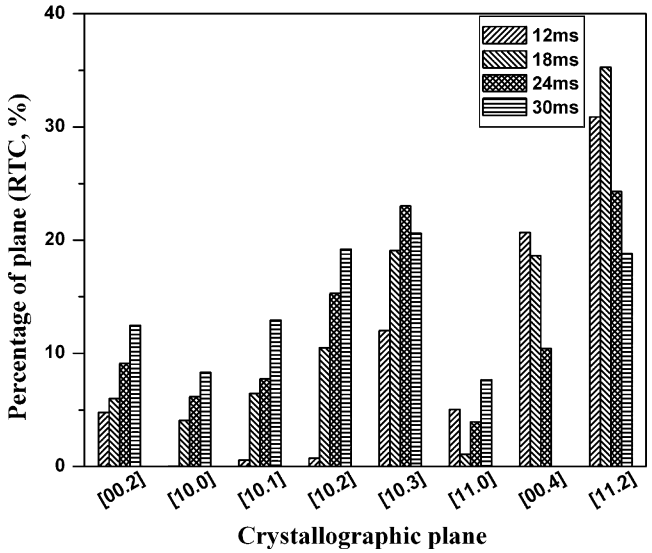

Fig. 13. Percentage RTC as a function of crystallographic planes at constant T_{OFF} (60.7 ms), I_P (5 Adm^{-2}) and different T_{ON} of (a) 12 ms, (b) 18 ms, (c) 24 ms, and (d) 30 ms.

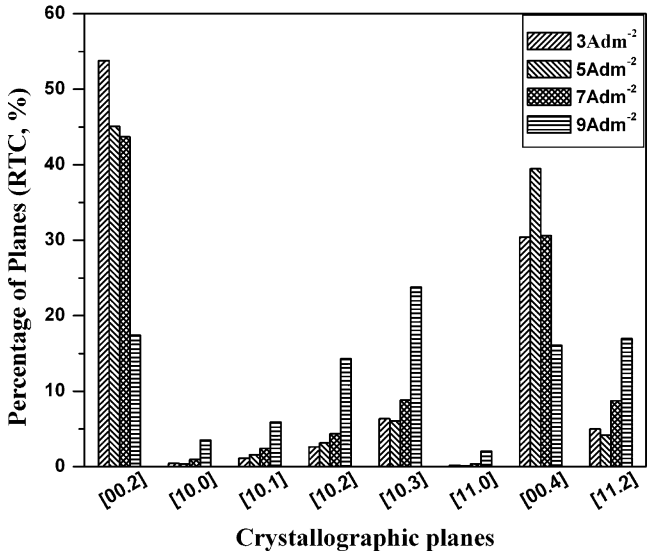

Fig. 14. Percentage RTC as a function of crystallographic planes at constant T_{ON} (6 ms), T_{OFF} (60.7 ms) and different I_P of (a) 3 Adm^{-2}, (b) 5 Adm^{-2}, (c) 7 Adm^{-2}, and (d) 9 Adm^{-2}.

Increasing T_{OFF} at constant T_{ON} and I_P exhibit prevailing basal [0 0. 2] texture compared to high angle pyramidal [1 0. 1], [1 1. 2] and prismatic [1 1. 0], [1 0. 0] planes (Fig. 12). The relative texture co-efficient (RTC, %) of [0 0. 2] increased from 10.3% at 18 ms (T_{OFF}) to 35.5% at 60.7 ms (T_{OFF}). According to the fundamental aspects discussed above, the zinc deposits with highest [0 0. 2] plane's RTC values exhibited significant low I_{corr} (22 μA cm^{-2}) and high R_{ct} (171.15 Ω cm^{-2}) values. Meanwhile, the T_{ON} variation tends to increase the I_{corr} and decrease R_{ct} values may be due to low RTC value of [0 0. 2] planes (Fig. 13) and low intensity oxide plane. The RTC values of [0 0. 2] planes increased significantly with increasing the I_P, along with drastic fall of I_{corr} values (Figs. 1c and 14) [34]. This is a due to surface energy differences, which are responsible, for the selective growth of the grains that have the lowest surface free energy. For the zinc crystal the lowest surface energy is the basal [0 0. 2] plane owing to its compactness [35].

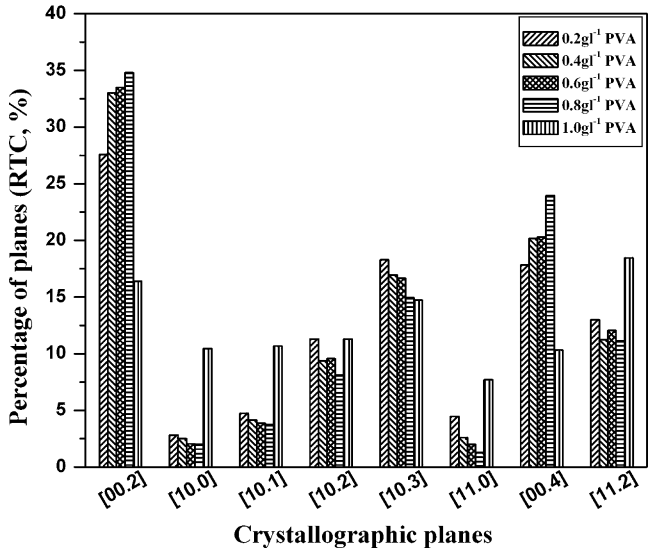

Fig. 15. Percentage RTC as a function of crystallographic planes at constant T_{ON} (6 ms), T_{OFF} (60.7 ms), I_P (5 Adm^{-2}) and different PVA concentrations of (a) 0.3 g l^{-1}, (b) 0.6 g l^{-1}, (c) 0.9 g l^{-1}, (d) 1.2 g l^{-1}, and (e) 1.5 g l^{-1}.

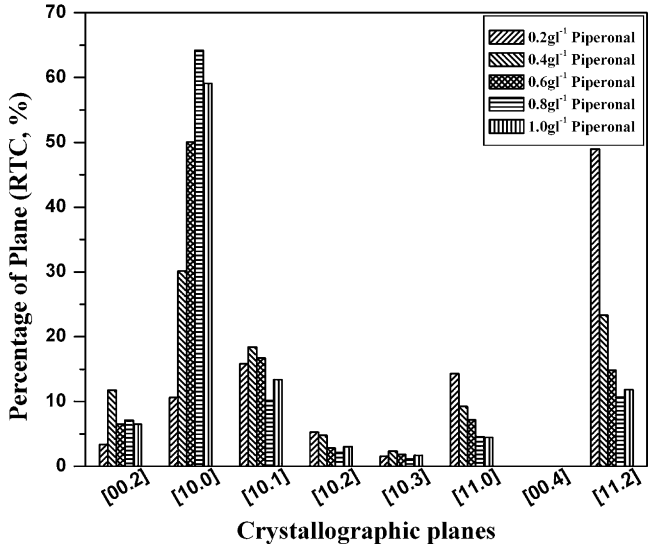

Fig. 16. Percentage RTC as a function of crystallographic planes at constant T_{ON} (6 ms), T_{OFF} (60.7 ms), I_P (5 Adm^{-2}), PVA concentration (0.9 g l^{-1}) and different piperonal concentrations of (a) 0.2 g l^{-1}, (b) 0.4 g l^{-1}, (c) 0.6 g l^{-1}, (d) 0.8 g l^{-1}, and (e) 1.0 g l^{-1}.

However, at 0.9 g l^{-1} PVA, zinc deposit contained about 80% of its crystallites preferably orientated to basal [0 0. 2] plane (Figs. 1d and 15) while only 10% of crystallites were orientated with inclusion of piperonal + 0.9 g l^{-1} PVA (Figs. 1e and 16). The remarkable decrease in RTC values of basal [0 0. 2] plane were due to increased overpotential [36] for zinc deposition and the decrease of grain size due to piperonal addition. But the deposits obtained at 0.4 g l^{-1} piperonal + 0.9 g l^{-1} PVA concentrations are 1.25 times more corrosion protective compared to those obtained with electrolyte containing only 0.9 g l^{-1} PVA, which contradict the above-mentioned aspects. Therefore, presences of additives modify the morphology, the crystal orientation and the surface roughness of deposited zinc which inturn have an effect on its corrosion property.

4. Conclusion

Application of pulse electrodeposition resulted in adherent and bright nanocrystalline zinc deposits with average grain size ranging from 30 to 50 nm from an alkaline non-cyanide electrolyte containing additives. The corrosion properties of pulsed zinc varied depending upon the plating conditions. I_{corr} decreased with increase in T_{OFF} and I_P (both with and without additives) and vice-versa for T_{ON} effect. Bright, compact and homogenous nanocrystalline zinc coating with best corrosion resistance of 16 $\mu A\,cm^{-2}$ (I_{corr}) was obtained at 6 ms (T_{ON}), 60.7 ms (T_{OFF}), 5 Adm^{-2} (I_P), 0.9 $g\,l^{-1}$ PVA + 0.4 $g\,l^{-1}$ piperonal concentrations. RTC values of zinc [0 0. 2] crystallographic plane vary with pulse parameters and additive concentrations and attribute enhance corrosion properties of zinc coatings. Therefore, pulse plating served as an agent for effective grain refinement, at moderate current densities enabling the preparation of compact and bright zinc deposits at less additives concentrations. The new bath also has the additional advantage of being eco-friendly in that it uses only easily disposable organics.

Acknowledgements

The authors wish to express their sincere thanks to the staff of Central Instrumentation facility for the support rendered in the study. M.S. Chandrasekar expresses his gratitude to CSIR, New Delhi for Diamond Jubilee Research Intern Scheme.

References

[1] K.S. Kumar, H. Van Swygenhoven, S. Suresh, Acta Mater. 51 (2003) 5743.
[2] L. Lu, Y. Shen, X. Chen, L. Qian, K. Lu, Science 304 (2004) 422.
[3] J. Schiotz, K.W. Jacobsen, Science 301 (2003) 1357.
[4] Y. Wang, M. Chen, F. Zhou, E. Ma, Nature 419 (2002) 912.
[5] A.J. Detor, C.A. Schuh, Acta Mater. 55 (2007) 371.
[6] L. Wang, J. Zhang, Y. Gao, Q. Xue, L. Hu, T. Xu, Scripta Mater. 55 (2006) 657.
[7] D.H. Jeong, F. Gonzalez, G. Palumbo, K.T. Aust, U. Erb, Scripta Mater. 44 (2001) 493.
[8] H.S. Kim, M.B. Bush, Nanostruct. Mater. 11 (1999) 361.
[9] A. Gomes, M.I. da Silva Pereira, Electrochim. Acta 51 (2006) 1342.
[10] Kh.M.S. Youssef, C.C. Koch, P.S. Fedkiw, Corros. Sci. 46 (2004) 51.
[11] R. Ramanauskas, L. Gudaviciute, R. Juskenas, O. Scit, Electrochim. Acta 53 (2007) 1801.
[12] R. Ramanauskas, L. Gudaviciute, O. Scit, D. Bucinskiene, R. Juskenas, Trans. Inst. Met. Finish. 86 (2008) 103.
[13] Shanmugasigamani, P. Malathy, J. Appl. Electrochem. 36 (2006) 315.
[14] M.S. Chandrasekar, Shanmugasigamani, P. Malathy, J. Solid State Electrochem. 13 (2009) 781.
[15] L. Oniciu, L. Muresan, J. Appl. Electrochem. 21 (1991) 265.
[16] V. Zuniga, R. Ortega, Y. Meas, G. Trejo, Plating Surf. Finish 91 (June) (2004).
[17] H. Nakano, S. Oue, T. Miki, S. Kobayashi, H. Fukushima, ISIJ Int. 46 (2006) 106.
[18] M.S. Chandrasekar, P. Malathy, Electrochim. Acta 53 (2008) 3313.
[19] Kh.M.S. Youssef, C.C. Koch, P.S. Fedkiw, J. Electrochem. Soc. 151 (2004) C103.
[20] M.S. Chandrasekar, Shanmugasigamani, P. Malathy, J. mater. Sci. 45 (2010) 1160.
[21] Kh. Saber, C.C. Koch, P.S. Fedkiw, Mater. Sci. Eng. A 341 (2003) 174.
[22] H. Geduld, Zincate or Alkaline Non-cyanide Zinc Plating in Zinc Plating, ASM International Metals Park, OH, 1988, p. 90.
[23] E. budman, Met. Finish. 93 (1995) 60.
[24] G.D. Wilcox, P.J. Mitchell, Trans. Inst. Met. Finish. 65 (1987) 76.
[25] L.Ph. Berube, G. L'Esperance, J. Electrochem. Soc. 136 (1989) 2314.
[26] A. Bai, P.-Y. Chuan, C.-C. Hu, Mater. Chem. Phys. 82 (2003) 93.
[27] H. Brown, Plating 3 (1968) 1047.
[28] S. Martin, US Patent No. 4,397,718.
[29] J.Cl. Puippe, Influence of pulse plating on crystallization, in: J.Cl. Puippe, F. Leaman (Eds.), Theory and Practice of Pulse Plating, AESF, Orlando, FL, 1986, p. 17.
[30] R.T.C. Choo, J.M. Toguri, A.M. El-Sherik, U. Erb, J. Appl. Electrochem. 25 (1995) 384.
[31] R.F. Ashton, M.P. Hepworth, Corrosion 24 (1968) 50.
[32] K.M. Youssef, C.C. Koch, P.S. Fedkiw, Electrochim. Acta 54 (2008) 677.
[33] C.J. Park, M.M. Lohrengel, T. Hamelmann, M. Pilaski, H.S. Kwon, Electrochim. Acta 47 (2002) 3395.
[34] D.Y. Li, J.A. Szpunar, Electrochim. Acta 42 (1997) 47.
[35] Z.A. matysina, L.M. Chuprina, S.Yu. Zaginoichenko, J. Phys. Chem. Solids 53 (1992) 167.
[36] N.A. Pangarov, J. Electroanal. Chem. 9 (1965) 70.